

Strong Spin-Motion Coupling in the Ultrafast Dynamics of Rydberg Atoms


V. Bharti^{1,*}, S. Sugawa^{1,2,3}, M. Kunimi⁴, V. S. Chauhan¹, T. P. Mahesh^{1,2}, M. Mizoguchi¹, T. Matsubara¹,
T. Tomita^{1,2}, S. de Léséleuc^{1,2,†} and K. Ohmori^{1,2,‡}

¹*Institute for Molecular Science, National Institutes of Natural Sciences, Okazaki 444-8585, Japan*

²*SOKENDAI (The Graduate University for Advanced Studies), Okazaki 444-8585, Japan*

³*Department of Basic Science, The University of Tokyo, Meguro-ku, Tokyo, 153-8902, Japan*

⁴*Department of Physics, Tokyo University of Science, Shinjuku-ku, Tokyo, 162-8601, Japan*

 (Received 20 November 2023; revised 19 April 2024; accepted 2 August 2024; published 30 August 2024)

Rydberg atoms in optical lattices and tweezers is now a well-established platform for simulating quantum spin systems. However, the role of the atoms' spatial wave function has not been examined in detail experimentally. Here, we show a strong spin-motion coupling emerging from the large variation of the interaction potential over the wave function spread. We observe its clear signature on the ultrafast many-body nanosecond-dynamics of atoms excited to a Rydberg S state, using picosecond pulses, from an unity-filling atomic Mott-insulator. We also propose an approach to tune arbitrarily the strength of the spin-motion coupling relative to the motional energy scale set by trapping potentials. Our work provides a new direction for exploring the dynamics of strongly correlated quantum systems by adding the motional degree of freedom to the Rydberg simulation toolbox.

DOI: [10.1103/PhysRevLett.133.093405](https://doi.org/10.1103/PhysRevLett.133.093405)

Quantum simulation platforms, such as ion crystals [1], polar molecules [2], ultracold neutral atoms [3], and Rydberg atoms [4], offer remarkable opportunities to study various many-body problems, of which one important category are localized spin models, see e.g., [5–9]. To mimic pure spin systems, two energy levels in the internal degrees of freedom (d.o.f.) are identified as an effective spin-1/2, and approximations are then applied onto the full Hamiltonian describing a given experimental platform, notably to decouple the external motional d.o.f. (position and momentum) from the spin dynamics. Recently, new proposals are emerging to purposely use *spin-motion coupling* (i.e., a state-dependent force) and open new regimes of quantum simulation with Rydberg atoms [10–15]. In this work, based on the ultrafast Rydberg quantum platform [16,17], we report on the experimental realization of an extreme regime of spin-motion coupling κ which is (i) comparable to the spin-spin interaction strength V , and (ii) overly dominates the natural motional energy scale ω set by a trapping potential. We also propose an experimental approach, *ultrafast stroboscopic Rydberg excitation*, to tune the ratio κ/ω over many orders of magnitude.

Rydberg atoms display interactions ranging up to the GHz-scale at micrometer interatomic distances r [4,18]. The potential $V(r)$ typically follows a $1/r^3$ -dependence for resonant dipole-dipole interaction, or a $1/r^6$ potential in the nonresonant van der Waals (vdW) regime. Over the last decade, spin models have been implemented with Rydberg atoms in a gas phase [19–21], in an optical lattice [17,22,23], or in an array of optical tweezers, e.g., [8,9,24,25]. In these works, spin-motion coupling (arising when the atom explores the spatially varying potential) is either considered negligible, or as a small source of decoherence with the external d.o.f. treated as a thermal bath. For example, if atoms move randomly during the dynamics, because of a finite thermal energy, the interaction varies and blurs the spin dynamics. By preparing atoms in a pure motional quantum state, the coupling to motion is coherent and creates spin-motion entanglement [16].

In this coherent regime, the spin-motion coupling originates from the variation of the potential $V(r)$ over the root mean squared (rms) spread x_{rms} of the atom position wave function, around a distance d [13]. The first-order, linear, spin-motion coupling term is parametrized by κ ,

$$\kappa = -x_{\text{rms}} \left. \frac{\partial V}{\partial x} \right|_{x=d} = 6 \frac{x_{\text{rms}}}{d} V(d), \quad (1)$$

where we assumed a repulsive vdW potential. First, we compare the ratio of spin-motion to spin-spin coupling κ/V , which depends on the choice of optical traps: lattice or tweezers. In both approaches, the quantum fluctuation of position $x_{\text{rms}} = \sqrt{\hbar/2m\omega}$ (m the mass of the atom) is

*Contact author: vineet.bharti@bristol.ac.uk

Present address: Quantum Engineering Technology Laboratories and School of Physics, University of Bristol, BS8 1TL, United Kingdom.

†Contact author: sylvain@ims.ac.jp

‡Contact author: ohmori@ims.ac.jp

slightly tunable through the trapping angular frequency $\omega \sim 2\pi \times 10\text{--}100$ kHz giving a spread of a few tens of nanometers. The distance d between atoms is typically $0.5\ \mu\text{m}$ with lattice and can range from 2 to $10\ \mu\text{m}$ for tweezers. Consequently, the spin-motion coupling is usually only a small perturbation for tweezers $\kappa/V \ll 0.1$ [16], while it is comparable to the spin-spin coupling in the lattice platform $\kappa/V \sim 0.5$. We will see clear signatures of this large perturbation on the spin dynamics in the first part of this work.

Second, we discuss the relevance of motion through the ratio κ/ω , which can vary over many orders of magnitude depending on the platform. For molecules, interacting through a dipole-dipole potential V on the kHz scale or less [6,26,27], the spin-motion coupling is negligible $\kappa/\omega < 0.01$, except if working with delocalized, overlapping, wave functions [28]. For Rydberg atoms excited with cw lasers, forcing the Rydberg blockade limits the interaction strength V to the MHz scale which nevertheless allows to enter the perturbative regime $\kappa/\omega \sim 0.1\text{--}0.5$ and already opens up exciting prospects [11–14]. By using picosecond pulsed lasers, our ultrafast approach allows to always overcome Rydberg blockade [29] and prepare Rydberg atoms with interaction strength at the GHz scale [16,17,19]. Here, the spin-motion coupling becomes overly dominant with $\kappa/\omega \sim 10\text{--}1000$, such that motional dynamics, due to the kinetic energy of atoms [30–32], can be completely neglected on the timescale of spin-spin and spin-motion entanglement. In the final part of this work, we will propose the ultrafast stroboscopic method to effectively tune κ/ω .

Experimental platform—The schematic of our experimental system is shown in Fig. 1(a). We prepare a three-dimensional (3D) unity-filling Mott-insulator state with $\sim 3 \times 10^4$ atoms in the $|\downarrow\rangle = |5S\rangle$ ground state of ^{87}Rb (electronic and nuclear spin d.o.f. are fully polarized and decoupled from the ultrafast dynamics). The 3D optical lattice, with period $a_{\text{lat}} = 532$ nm, has a depth of $20E_R$ for each axis giving rise to an isotropic trapping frequency $\omega = 2\pi \times 18$ kHz in the harmonic oscillator approximation [17]. The spatial wave function $|\psi\rangle_{\text{spatial}}$ of each atom, prepared in the motional ground state of each lattice site, have a quantum uncertainty of position $x_{\text{rms}} = 57$ nm, and a momentum uncertainty $p_{\text{rms}} = \hbar/2x_{\text{rms}} = m \times (6.4\ \text{mm/s})$.

Following preparation of the ground-state atoms, they are then coherently excited to the $|\uparrow\rangle = |29S\rangle$ Rydberg state using a two-photon (779 and 483 nm) off-resonant excitation with broadband laser pulses (~ 10 ps duration) as described in Ref. [33] and shown in Fig. 1(b). This prepares each atom in a coherent electronic superposition $|\psi\rangle_{\text{elec}} = \sqrt{1-p}|\downarrow\rangle + \sqrt{p}|\uparrow\rangle$, with p the probability to be in the Rydberg state, typically 4%–6% [17,19], and where we mapped the ground and Rydberg states to a spin 1/2. Two atoms in the $29S$ state experience strong dipole-dipole

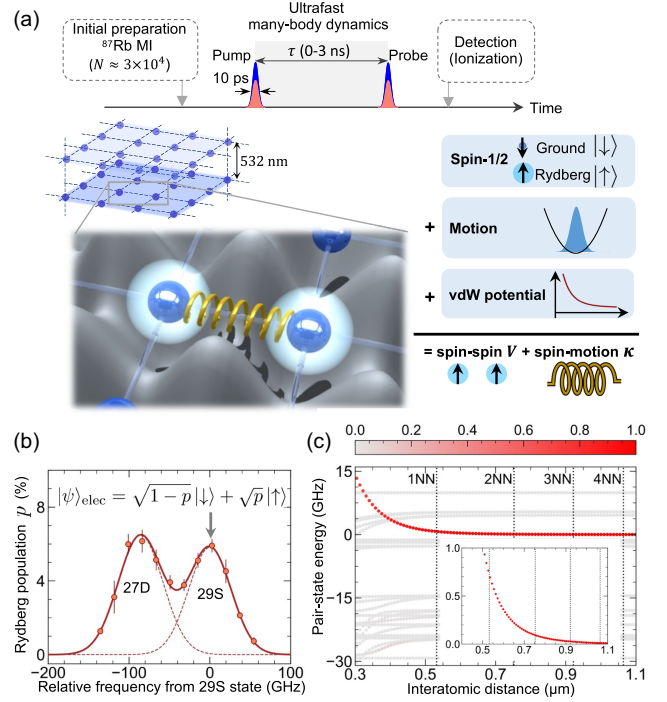


FIG. 1. (a) Schematic of the experiment. The atoms prepared in a unity-filling 3D atomic Mott-insulator are coherently excited to the $29S$ Rydberg state using a pump pulse. After the pump excitation, the system undergoes many-body dynamics driven by spin-spin and spin-motion couplings until the probe pulse is applied. (b) Rydberg state population after pump excitation. The solid curve shows a fit by a double Gaussian function, while the dashed curves represents the individual contribution from the state $27D$ and $29S$. At resonance, the population in $27D$ state is only $\sim 0.2\%$. (c) The $29S - 29S$ pair state energy as a function of inter-atomic distance. The inset zooms in the $0\text{--}1$ GHz energy range.

interaction in the vdW regime. Figure 1(c) shows the interaction potential calculated using the pairinteraction software [34,35]. It is very well approximated by an isotropic, repulsive, vdW form $V(r) = C_6/r^6$, where the calculated coefficient C_6^{th} is $2\pi \times 16\ \text{MHz}\ \mu\text{m}^6$. The mixing with the dominant interaction channel (the pair-state $28P - 29P$) remains negligible thanks to its large energy separation of 20 GHz. Choosing a Rydberg S state, rather than D state as in previous works [16,17], was motivated by obtaining this clean isotropic potential, despite the increased experimental challenge caused by the smaller excitation strength of S state and in spectrally resolving the S and D states when using picosecond laser pulses [33].

The model Hamiltonian—Here, we discuss the model Hamiltonian, including the motional d.o.f. Following excitation, each atom j is initially in a product state of spatial and internal d.o.f. $|\psi_j\rangle = |\psi\rangle_{\text{spatial}} \otimes |\psi\rangle_{\text{elec}}$. We then consider the evolution of this system in the nanosecond timescale relevant for spin-spin and spin-motion entanglement. For such short duration, the motion of atoms can be completely ignored: the position probability

distribution do not have time to evolve either from the absence of confining potential for the Rydberg state or from the vdW repulsion. The ultrafast dynamics is then driven only by

$$\begin{aligned} \frac{\hat{H}}{\hbar} &= \sum_{j < k} V(\hat{\mathbf{r}}_{jk}) \otimes \hat{n}_j \hat{n}_k \\ &\approx \sum_{j < k} \left(V_{jk} + \kappa_{jk} \frac{\hat{\mathbf{r}}_{jk} - \bar{\mathbf{r}}_{jk}}{x_{\text{rms}}} \cdot \mathbf{e}_{jk} + \dots \right) \otimes \hat{n}_j \hat{n}_k. \end{aligned} \quad (2)$$

Here, $\hat{\mathbf{r}}_{jk} = \hat{\mathbf{r}}_j - \hat{\mathbf{r}}_k$ is the quantum operator of the relative position of atoms j and k , $\bar{\mathbf{r}}_{jk}$ its expectation value, \mathbf{e}_{jk} a unit vector along site j and k , V_{jk} and κ_{jk} the couplings evaluated at distance \bar{r}_{jk} , and $\hat{n}_j = |\uparrow\rangle_j \langle \uparrow|$ is the projection operator on the Rydberg state for the j th atom. Applying this Hamiltonian to the initial product state creates entanglement within the spin sector, but also, and this is the key point of the first part of this work, between the spin and motional sectors of the Hilbert space.

Results—We now present experimental results obtained by time-domain Ramsey interferometry [16,17,19] with $p \sim 4.8\%$, to probe the many-body entangled state generated by the above Hamiltonian. In short, a first pump pulse initiates the many-body dynamics which is read out by a second probe pulse after a variable delay $\tau = 0\text{--}3$ ns. This second pulse gives rise to a Ramsey interference whose contrast is a probe to the single-atom coherence in the spin sector, i.e., between the ground and Rydberg state. Spin-spin and spin-motion coupling generates entanglement entropy [17], which reduces the single-atom coherence and thus the Ramsey contrast. Ramsey interferograms are obtained by measuring the Rydberg population p after the probe pulse, as a function of relative pump-probe delay, by detecting the field-ionized Rydberg atoms using a microchannel plate [33]. Typical interferograms are shown in Figs. 2(a) and 2(b). In absence of interaction (blue curve, obtained for a low-density atomic sample), the highly contrasted interference indicates a constant pure state. For atoms prepared as a Mott-insulator (red curve), the decreasing contrast signals a reduced purity in the spin sector, which is shown in Fig. 2(c) as a function of the delay τ . Additionally, we also extract a phase shift of the Ramsey oscillations with the reference noninteracting sample.

Numerical solution—To calculate the Ramsey contrast and phase shift from the action of the Hamiltonian of Eq. (2), we extend previous results [19,36] to include the spatial wavefunction of each atom, which requires to calculate terms such as the two-body spatial overlap:

$$\begin{aligned} O_{jk}(t) &= \langle \psi_j; \psi_k | \exp(-iV(\hat{\mathbf{r}})t) | \psi_j; \psi_k \rangle \\ &= C \int d\mathbf{r} \exp\left(-\frac{|\mathbf{r} - \bar{\mathbf{r}}_{jk}|^2}{x_{\text{rms}}^2} - i \frac{C_6}{|\mathbf{r}|^6} t\right), \end{aligned} \quad (3)$$

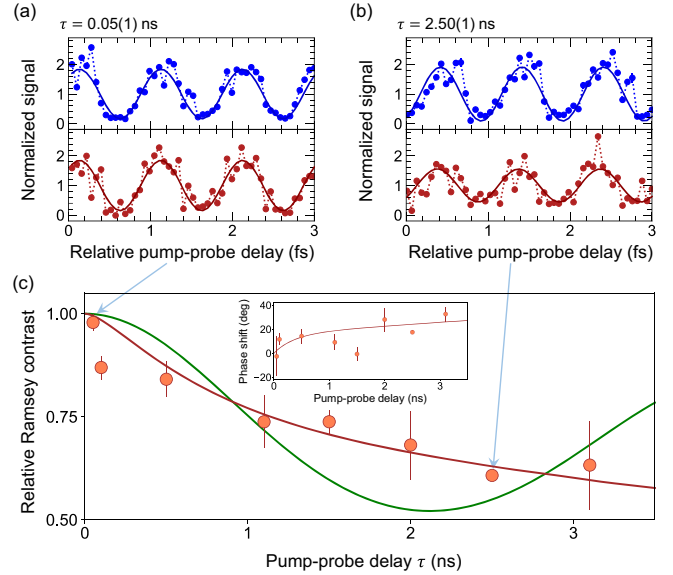


FIG. 2. Time-domain Ramsey interferograms for atoms prepared in a Mott insulator, strongly interacting, state (red) and a low-density, noninteracting, reference atomic sample (blue) for (a) $\tau = 0.05$ and (b) $\tau = 2.5$ ns. The vertical axis of each interferogram is normalized by the mean value of data. (c) Measured relative Ramsey contrasts (ratio of the contrasts of Mott-insulator and reference sample) and phase shifts (phase difference of Mott-insulator and reference sample) are shown by red circles (error bars are standard error of the mean). The observations are compared with a fitted numerical solution that takes into account spin-motion coupling (red curve) or ignore it (green curve).

where C is a normalization constant. The second line is obtained after reformulating the two-body wavefunctions $|\psi_j; \psi_k\rangle$ into two independent one-body system: a trivial one for the center-of-mass, unaffected by the interaction, and the interesting one for the relative coordinate \mathbf{r}_{jk} with reduced mass $m/2$. For a two-atom system, the Ramsey contrast and phase are directly related to the amplitude and phase of the complex-valued overlap O . For the many-body dynamics considered here, the analytical expression relating them is given in Ref. [33], which also include details on neglecting three-body (and higher) overlap terms.

The calculation results are then fitted to the relative Ramsey contrast data with a single free parameter: the coefficient C_6 . The fitted curve, see Fig. 2(c), agrees well with the experimental data for a coefficient $C_6^{\text{exp}} = 2\pi \times 5.5 \text{ MHz } \mu\text{m}^6$. With this value, the positive trend (related to the sign of C_6) and magnitude of the phase shift are also well captured. The fitted C_6^{exp} coefficient is 3 times smaller than obtained from ab-initio calculation of the vdW potential, which calls for further investigation of the accuracy of the vdW potential calculation in the short, submicron distance regime. This could be done using a tweezers platform where a simpler system of only two atoms can be prepared [16], potentially down to the short sub-micrometer distance by throwing atoms with moving tweezers [37].

To emphasize the importance of the spin-motion coupling in this experiment, we also show calculation for a pure spin-spin model where we ignore the spatial extent of the wave functions [17,19]. As shown in the green curve of Fig. 2(c), the Ramsey contrast would have displayed an oscillation (see *Discussion*) which is clearly absent in the experimental data. We can thus conclude that capturing spin-motion entanglement is essential to account for the observed many-body dynamics.

Discussion—We now present a hierarchy of approximations to identify the relevant terms in Eqs. (2) and (3) that create spin-motion entanglement. We consider two atoms at nearest-neighbor (NN) distance a_{lat} , where the variation of potential over the wave function describing their relative distance $\psi_{12}(\mathbf{r})$ is largest. We then restrict the problem to one dimension, along the interatomic axis, by neglecting the wave function spread in the other two directions as it gives a small $\frac{1}{2}(x_{\text{rms}}/a_{\text{lat}})^2 \simeq 0.5\%$ increase in NN distance, 20 times smaller than the effect along the interatomic axis. This allows a phase-space representation of the 1D wave function $\psi_{12}(x)$, as shown in Fig. 3(a), which is convenient to depict the relative motional states of two atoms with the Rydberg interaction [14].

The $1/r^6$ potential then applies a strong force on the wavefunction which can be decomposed with a series expansion of the potential around the mean interatomic distance a_{lat} . The zeroth-order term $V = C_6^{\text{exp}}/a_{\text{lat}}^6$ gives rise to spin-spin entanglement reaching its maximal value at time $\tau = \pi/V = 2.1$ ns, and corresponding to a minimum in the Ramsey contrast of the green curve of Fig. 2(c). For longer time, the two effective spins would de-entangle and the Ramsey visibility restore [16,38]. The first-order linear term, explicitly written in Eq. (2), gives a uniform force on the wavefunction $F = 6\hbar C_6/a_{\text{lat}}^7 = \hbar\kappa/x_{\text{rms}} \simeq (m/2)(2.5 \times 10^7 \text{ m s}^{-2})$. The momentum kick Δp from this acceleration becomes comparable to the relative momentum rms spread after $\tau = p_{\text{rms}}/\sqrt{2}F = 0.3$ ns. As the state-dependent force is applied only on part of the spin sector ($|\uparrow\uparrow\rangle$), it creates spin-motion entanglement that is captured by the reduced overlap $|O|$ between the displaced and initial momentum wave function seen in Fig. 3(b). It explains why the Ramsey contrast drops initially faster than expected from a pure spin model, see Fig. 2(c), as well as why it does not restore beyond $\tau = 2.1$ ns as the pure spin model predicts.

For a good qualitative description of the dynamics, it is necessary to go beyond the first-order term to capture the wide variation of the mechanical force over the wave function. As seen in Fig. 3(b), a second-order expansion brings the calculated overlap much closer to the exact result from Eq. (3). Qualitatively, these second-order terms $\hat{r}_{jk}^2 = (\hat{x}_j - \hat{x}_k)^2$ have two interesting effects on the wave function. First, they squeeze each atom wave function through the terms \hat{x}_j^2 and \hat{x}_k^2 : the atoms feel a stronger force at

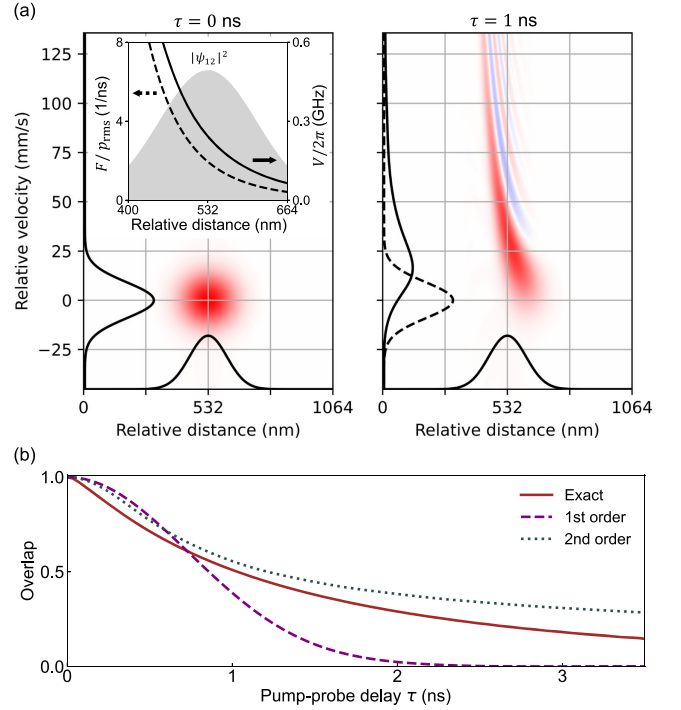


FIG. 3. (a) Phase-space (Wigner) representation of the relative wave function ψ_{12} at time $\tau = 0$ and 1 ns. The ψ_{12} at $\tau = 0$ ns is the relative wave function of the two atoms in the motional ground state of the lattice sites. The red (blue) color represents positive (negative) value of the Wigner distribution. The marginal position and velocity distribution are shown as black lines. The momentum displacement and squeezing are clearly visible. Inset: zoom on the probability distribution $|\psi_{12}|^2$, showing the spatial variation of the vdW potential V (solid), and the resulting force F (dashed). (b) Overlap $|O(t)|$ as a function of the delay τ . Solid curve: exact calculation of Eq. (3). The dashed (dotted) lines are obtained by expanding the vdW potential to first order (second order).

shorter distance from the other one, which will compress the wave function. And second, they entangle the two atoms wave functions through the cross term $\hat{x}_j\hat{x}_k$. The relative wave function ψ_{12} cannot anymore be decomposed into a product state of two single-atom wave functions. Such entanglement between the motion of two atoms is not captured at lower order. The third-order terms are required to explain the negative value taken by the Wigner distribution.

Outlook—The strong spin-motion coupling observed here precludes the realization of a pure spin model in our experimental regime. However, instead of performing quantum simulation in the spin sector, we could rather work fully in the motion sector of the Hilbert space. This would be realized by completely transferring ground-state atoms to Rydberg orbits, a step that can be done with high-fidelity in the microsecond timescale [39] (but only for weakly interacting atoms), and for which progress have been reported by our group for picosecond-scale excitation [16].

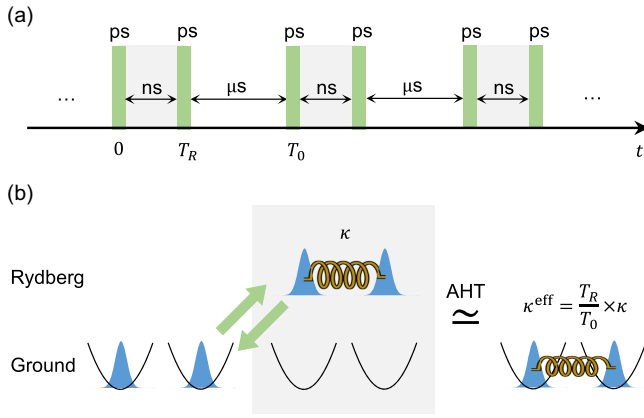


FIG. 4. Hamiltonian engineering by *ultrafast stroboscopic Rydberg excitation*. (a) Pulse sequence, see text. (b) The stroboscopic sequence gives rise to an average Hamiltonian with tunable interaction strength competing with the trapping potential.

We could then prepare a unit-filling Mott-insulator state of *Rydberg* atoms which would be submitted to strong internal vdW force [40]. Interestingly, the forces from two opposite directions of a given atom cancel in first-order and the second-order squeezing and entangling terms would dominate the dynamics. This would lead to nontrivial distortion of the spatial wave functions observable by time-of-flight imaging, a technique also available on the tweezers platform [41,42].

In this work, we neglected the effect of kinetic energy due to the large separation of timescales between the Rydberg interaction (nanoseconds) and the motion of atoms (microseconds). We now propose to bring these two scales together to investigate a larger class of Hamiltonians with *ultrafast stroboscopic Rydberg excitation*. As schematically drawn in Fig. 4, ground-state atoms are transferred in a picosecond timescale to Rydberg states to experience for a brief time T_R the strong force demonstrated in this work. This gives a momentum kick that can be widely tuned, by T_R and the choice of Rydberg state, with respect to the trap depth (we should not kick atoms out of their trapping sites). They are then brought back to the ground-state to now experience the kinetic energy and the trapping potential on a microsecond-timescale T_0 . This step is repeated with a high enough frequency to apply Average Hamiltonian Theory (AHT) [43–46], and a controlled duty cycle to vary the effective, reduced, coupling strength $\kappa_{\text{eff}} = T_R/T_0 \times \kappa$ relatively to the trapping frequency ω . Optionally, a spin-1/2 can be encoded in the ground-state manifold, and a spin-dependent force obtained by spin-selective ultrafast excitation. We note that this requires to combine ultrafast excitation with resolving the $6.8 \text{ GHz} = 1/(150 \text{ ps})$ hyperfine splitting, which is one of our ongoing developments.

This ultrafast Floquet engineering approach can be seen as complementary to Rydberg dressing [20,22,25,47–49],

where a trapped ground-state atom is instead continuously and weakly dressed by a small fraction of Rydberg character. Compared to other proposals for spin-motion coupling using long-lived circular Rydberg states [14], or Rydberg facilitation (antiblockade) [11–13], here we note that the stroboscopic approach has the practical advantage to not require magic-trapping of the Rydberg state. Finally, we emphasize that ultrafast Rydberg excitation with pulsed lasers (delivering up to 100 GHz of ground-Rydberg Rabi frequency) unlocks the full GHz-strength of interaction between Rydberg atoms, otherwise curbed by the limited MHz-scale Rabi frequency achievable with cw lasers.

In conclusion, we have considered the force experienced by Rydberg atoms, mapped it into a spin-motion coupling term, and observed a clear signature: a strong perturbation to the spin dynamics. We proposed a quantum control technique, ultrafast Floquet engineering, to tune the relative strength of this force compared to the trapping potential of optical lattice or tweezers, opening regimes of quantum simulation with Rydberg atoms. Among the new avenues, we envision the creation of exotic motional states such as a Rydberg crystal: an atomic array with each atom stabilized in free-space (i.e., in the absence of a confining lattice potential) by long-range isotropic vdW repulsion between Rydberg atoms, a state reminiscent of electronic Wigner crystals [50].

Note added—Recently, we became aware of related work on spin-motion entanglement that demonstrates quantum information processing using motional d.o.f. in tweezers [51].

Acknowledgments—The authors acknowledge Y. Okano and H. Chiba for the technical support. We thank E. Braun, H. Tamura, A. Trautmann, S. Weber, and C. A. Weidner for fruitful discussions; and Y. Zhang for the helpful discussions regarding the extension of delay line. This work was supported by MEXT Quantum Leap Flagship Program (MEXT Q-LEAP) JPMXS0118069021, JSPS Grant-in-Aid for Specially Promoted Research Grant No. 16H06289 and JST Moonshot R&D Program Grant No. JPMJMS2269. S. S. acknowledges support from JSPS KAKENHI Grant No. JP21H01021. M. K. acknowledges supports from JSPS KAKENHI Grants No. JP20K14389 and No. JP22H05268.

- [1] C. Monroe, W. C. Campbell, L.-M. Duan, Z.-X. Gong, A. V. Gorshkov, P. W. Hess, R. Islam, K. Kim, N. M. Linke, G. Pagano, P. Richerme, C. Senko, and N. Y. Yao, Programmable quantum simulations of spin systems with trapped ions, *Rev. Mod. Phys.* **93**, 025001 (2021).
- [2] T. Langen, G. Valtolina, D. Wang, and J. Ye, Quantum state manipulation and science of ultracold molecules, *Nat. Phys.* **20**, 702 (2024).
- [3] C. Gross and I. Bloch, Quantum simulations with ultracold atoms in optical lattices, *Science* **357**, 995 (2017).

- [4] A. Browaeys and T. Lahaye, Many-body physics with individually controlled Rydberg atoms, *Nat. Phys.* **16**, 132 (2020).
- [5] M. K. Joshi, F. Kranzl, A. Schuckert, I. Lovas, C. Maier, R. Blatt, M. Knap, and C. F. Roos, Observing emergent hydrodynamics in a long-range quantum magnet, *Science* **376**, 720 (2022).
- [6] B. Yan, S. A. Moses, B. Gadway, J. P. Covey, K. R. Hazzard, A. M. Rey, D. S. Jin, and J. Ye, Observation of dipolar spin-exchange interactions with lattice-confined polar molecules, *Nature (London)* **501**, 521 (2013).
- [7] P. N. Jepsen, J. Amato-Grill, I. Dimitrova, W. W. Ho, E. Demler, and W. Ketterle, Spin transport in a tunable Heisenberg model realized with ultracold atoms, *Nature (London)* **588**, 403 (2020).
- [8] G. Semeghini, H. Levine, A. Keesling, S. Ebadi, T. T. Wang, D. Bluvstein, R. Verresen, H. Pichler, M. Kalinowski, R. Samajdar, A. Omran, S. Sachdev, A. Vishwanath, M. Greiner, V. Vuletić, and M. D. Lukin, Probing topological spin liquids on a programmable quantum simulator, *Science* **374**, 1242 (2021).
- [9] C. Chen, G. Bornet, M. Bintz, G. Emperauger, L. Leclerc, V. S. Liu, P. Scholl, D. Barredo, J. Hauschild, S. Chatterjee, M. Schuler, A. M. Läuchli, M. P. Zaletel, T. Lahaye, N. Y. Yao, and A. Browaeys, Continuous symmetry breaking in a two-dimensional Rydberg array, *Nature (London)* **616**, 691 (2023).
- [10] R. Belyansky, J. T. Young, P. Bienias, Z. Eldredge, A. M. Kaufman, P. Zoller, and A. V. Gorshkov, Nondestructive cooling of an atomic quantum register via state-insensitive Rydberg interactions, *Phys. Rev. Lett.* **123**, 213603 (2019).
- [11] F. M. Gabbetta, W. Li, F. Schmidt-Kaler, and I. Lesanovsky, Engineering nonbinary Rydberg interactions via phonons in an optical lattice, *Phys. Rev. Lett.* **124**, 043402 (2020).
- [12] P. P. Mazza, R. Schmidt, and I. Lesanovsky, Vibrational dressing in kinetically constrained Rydberg spin systems, *Phys. Rev. Lett.* **125**, 033602 (2020).
- [13] M. Magoni, R. Joshi, and I. Lesanovsky, Molecular dynamics in Rydberg tweezer arrays: Spin-phonon entanglement and Jahn-Teller effect, *Phys. Rev. Lett.* **131**, 093002 (2023).
- [14] P. Méhaignerie, C. Sayrin, J.-M. Raimond, M. Brune, and G. Roux, Spin-motion coupling in a circular-Rydberg-state quantum simulator: Case of two atoms, *Phys. Rev. A* **107**, 063106 (2023).
- [15] Z. Zhang, M. Yuan, B. Sundar, and K. R. Hazzard, Motional decoherence in ultracold Rydberg atom quantum simulators of spin models, *arXiv:2201.08463*.
- [16] Y. Chew, T. Tomita, T. P. Mahesh, S. Sugawa, S. de Léséleuc, and K. Ohmori, Ultrafast energy exchange between two single Rydberg atoms on the nanosecond time-scale, *Nat. Photonics* **16**, 724 (2022).
- [17] V. Bharti, S. Sugawa, M. Mizoguchi, M. Kunimi, Y. Zhang, S. de Léséleuc, T. Tomita, T. Franz, M. Weidemüller, and K. Ohmori, Picosecond-scale ultrafast many-body dynamics in an ultracold Rydberg-excited atomic Mott insulator, *Phys. Rev. Lett.* **131**, 123201 (2023).
- [18] M. Saffman, T. G. Walker, and K. Mølmer, Quantum information with Rydberg atoms, *Rev. Mod. Phys.* **82**, 2313 (2010).
- [19] N. Takei, C. Sommer, C. Genes, G. Pupillo, H. Goto, K. Koyasu, H. Chiba, M. Weidemüller, and K. Ohmori, Direct observation of ultrafast many-body electron dynamics in an ultracold Rydberg gas, *Nat. Commun.* **7**, 13449 (2016).
- [20] V. Borish, O. Markovic, J. A. Hines, S. V. Rajagopal, and M. Schleier-Smith, Transverse-field Ising dynamics in a Rydberg-dressed atomic gas, *Phys. Rev. Lett.* **124**, 063601 (2020).
- [21] A. Signoles, T. Franz, R. Ferracini Alves, M. Gärtner, S. Whitlock, G. Zürn, and M. Weidemüller, Glassy dynamics in a disordered Heisenberg quantum spin system, *Phys. Rev. X* **11**, 011011 (2021).
- [22] J. Zeiher, R. Van Bijnen, P. Schauß, S. Hild, J.-y. Choi, T. Pohl, I. Bloch, and C. Gross, Many-body interferometry of a Rydberg-dressed spin lattice, *Nat. Phys.* **12**, 1095 (2016).
- [23] E. Guardado-Sanchez, P. T. Brown, D. Mitra, T. Devakul, D. A. Huse, P. Schauß, and W. S. Bakr, Probing the quench dynamics of antiferromagnetic correlations in a 2D quantum Ising spin system, *Phys. Rev. X* **8**, 021069 (2018).
- [24] K. Kim, F. Yang, K. Mølmer, and J. Ahn, Realization of an extremely anisotropic Heisenberg magnet in Rydberg atom arrays, *Phys. Rev. X* **14**, 011025 (2024).
- [25] L.-M. Steinert, P. Osterholz, R. Eberhard, L. Festa, N. Lorenz, Z. Chen, A. Trautmann, and C. Gross, Spatially tunable spin interactions in neutral atom arrays, *Phys. Rev. Lett.* **130**, 243001 (2023).
- [26] C. M. Holland, Y. Lu, and L. W. Cheuk, On-demand entanglement of molecules in a reconfigurable optical tweezer array, *Science* **382**, 1143 (2023).
- [27] Y. Bao, S. S. Yu, L. Anderegg, E. Chae, W. Ketterle, K.-K. Ni, and J. M. Doyle, Dipolar spin-exchange and entanglement between molecules in an optical tweezer array, *Science* **382**, 1138 (2023).
- [28] J.-R. Li, K. Matsuda, C. Miller, A. N. Carroll, W. G. Tobias, J. S. Higgins, and J. Ye, Tunable itinerant spin dynamics with polar molecules, *Nature (London)* **614**, 70 (2023).
- [29] M. Mizoguchi, Y. Zhang, M. Kunimi, A. Tanaka, S. Takeda, N. Takei, V. Bharti, K. Koyasu, T. Kishimoto, D. Jaksch, A. Glaetzle, M. Kiffner, G. Masella, G. Pupillo, M. Weidemüller, and K. Ohmori, Ultrafast creation of overlapping Rydberg electrons in an atomic BEC and Mott-insulator lattice, *Phys. Rev. Lett.* **124**, 253201 (2020).
- [30] T. Amthor, M. Reetz-Lamour, S. Westermann, J. Denskat, and M. Weidemüller, Mechanical effect of van der Waals interactions observed in real time in an ultracold Rydberg gas, *Phys. Rev. Lett.* **98**, 023004 (2007).
- [31] T. Amthor, M. Reetz-Lamour, C. Giese, and M. Weidemüller, Modeling many-particle mechanical effects of an interacting Rydberg gas, *Phys. Rev. A* **76**, 054702 (2007).
- [32] C. Ates, A. Eisfeld, and J. M. Rost, Motion of Rydberg atoms induced by resonant dipole-dipole interactions, *New J. Phys.* **10**, 045030 (2008).
- [33] See Supplemental Material at <http://link.aps.org/supplemental/10.1103/PhysRevLett.133.093405> for more details.
- [34] S. Weber, C. Tresp, H. Menke, A. Urvoy, O. Firstenberg, H. P. Büchler, and S. Hofferberth, Calculation of Rydberg interaction potentials, *J. Phys. B* **50**, 133001 (2017).

- [35] N. Šibalić, J. Pritchard, C. Adams, and K. Weatherill, ARC: An open-source library for calculating properties of alkali Rydberg atoms, *Comput. Phys. Commun.* **220**, 319 (2017).
- [36] C. Sommer, G. Pupillo, N. Takei, S. Takeda, A. Tanaka, K. Ohmori, and C. Genes, Time-domain Ramsey interferometry with interacting Rydberg atoms, *Phys. Rev. A* **94**, 053607 (2016).
- [37] H. Hwang, A. Byun, J. Park, S. de Léséleuc, and J. Ahn, Optical tweezers throw and catch single atoms, *Optica* **10**, 401 (2023).
- [38] H. Jo, Y. Song, M. Kim, and J. Ahn, Rydberg atom entanglements in the weak coupling regime, *Phys. Rev. Lett.* **124**, 033603 (2020).
- [39] H. Levine, A. Keesling, A. Omran, H. Bernien, S. Schwartz, A. S. Zibrov, M. Endres, M. Greiner, V. Vuletić, and M. D. Lukin, High-fidelity control and entanglement of Rydberg-atom qubits, *Phys. Rev. Lett.* **121**, 123603 (2018).
- [40] R. Faoro, C. Simonelli, M. Archimi, G. Masella, M. M. Valado, E. Arimondo, R. Mannella, D. Ciampini, and O. Morsch, van der Waals explosion of cold Rydberg clusters, *Phys. Rev. A* **93**, 030701(R) (2016).
- [41] A. Bergschneider, V.M. Klinkhamer, J.H. Becher, R. Klemt, L. Palm, G. Zürn, S. Jochim, and P.M. Preiss, Experimental characterization of two-particle entanglement through position and momentum correlations, *Nat. Phys.* **15**, 640 (2019).
- [42] M. Brown, S. Muleady, W. Dworschack, R. Lewis-Swan, A. Rey, O. Romero-Isart, and C. Regal, Time-of-flight quantum tomography of an atom in an optical tweezer, *Nat. Phys.* **19**, 569 (2023).
- [43] U. Haeberlen and J. S. Waugh, Coherent averaging effects in magnetic resonance, *Phys. Rev.* **175**, 453 (1968).
- [44] N. Goldman and J. Dalibard, Periodically driven quantum systems: Effective Hamiltonians and engineered gauge fields, *Phys. Rev. X* **4**, 031027 (2014).
- [45] A. Eckardt and E. Anisimovas, High-frequency approximation for periodically driven quantum systems from a Floquet-space perspective, *New J. Phys.* **17**, 093039 (2015).
- [46] J. Choi, H. Zhou, H. S. Knowles, R. Landig, S. Choi, and M. D. Lukin, Robust dynamic Hamiltonian engineering of many-body spin systems, *Phys. Rev. X* **10**, 031002 (2020).
- [47] Y.-Y. Jau, A. Hankin, T. Keating, I.H. Deutsch, and G. Biedermann, Entangling atomic spins with a Rydberg-dressed spin-flip blockade, *Nat. Phys.* **12**, 71 (2016).
- [48] E. Guardado-Sanchez, B.M. Spar, P. Schauss, R. Belyansky, J.T. Young, P. Bienias, A.V. Gorshkov, T. Iadecola, and W.S. Bakr, Quench dynamics of a Fermi gas with strong nonlocal interactions, *Phys. Rev. X* **11**, 021036 (2021).
- [49] J. A. Hines, S. V. Rajagopal, G. L. Moreau, M. D. Wahrman, N. A. Lewis, O. Markovic, and M. Schleier-smith, Spin squeezing by Rydberg dressing in an array of atomic ensembles, *Phys. Rev. Lett.* **131**, 063401 (2023).
- [50] E. Wigner, On the interaction of electrons in metals, *Phys. Rev.* **46**, 1002 (1934).
- [51] P. Scholl, A. L. Shaw, R. Finkelstein, R. B.-S. Tsai, J. Choi, and M. Endres, Erasure-cooling, control, and hyperentanglement of motion in optical tweezers, [arXiv:2311.15580](https://arxiv.org/abs/2311.15580).